

## Determination of seismic site classification of seismic recording stations in the Himalayan region using HVSR method



P. Anbazhagan<sup>a,b,\*</sup>, K.N. Srilakshmi<sup>a</sup>, Ketan Bajaj<sup>a</sup>, Sayed S.R. Moustafa<sup>b,c</sup>, Nassir S.N. Al-Arifi<sup>b</sup>

<sup>a</sup> Department of Civil Engineering, Indian Institute of Science, Bangalore 560012, India

<sup>b</sup> Geology and Geophysics Department, Faculty of Science, King Saud University, Riyadh 11451, Saudi Arabia

<sup>c</sup> Seismology Department, National Research Institute of Astronomy and Geophysics (NRIAG), Cairo 11421, Egypt

### ARTICLE INFO

#### Keywords:

Ground motion  
Seismic station  
Site class  
H/V ratio  
 $V_{S30}$

### ABSTRACT

An attempt has been made to classify seismic stations installed along the Himalayan belt and in adjoining regions using recorded strong-motion data and different empirical methods. For all recorded data, HVSRs (horizontal-to-vertical spectral ratios) were computed using pseudo-response spectral acceleration (PSA) values. Five empirical techniques based on HVSRs and PSA were used to classify the stations. The first and second methods are based on the predominant period of the site and relationship between  $V_{S30}$  and parameters of HVSR. The third and fourth methods compute the correlation between the HVSR curve of a station and standard HVSR curves. Fifth used the PSA and PGA (peak ground acceleration) to identify the site as rock and soil. Conclusively, the site class which had the highest frequency of occurrence amongst the five methods was determined to be the final class for a given station. The final site class recommended is matched with the existing available site classification and also with available field test results.

### 1. Introduction

Local geology and site conditions have a significant effect on the characteristics of ground motion. These local site conditions amplify the seismic motion during different time periods, and amplification is a key parameter in estimating structural damage. Therefore, the detailed study of site classification and site amplification is a matter of great importance in an earthquake-prone area. Site classification in terms of time average shear-wave velocity up to 30 m ( $V_{S30}$ ) has been adopted as an international standard for seismic site classification. Geophysical testing and drilling of boreholes are the reliable methods to obtain the detailed site-specific information of dynamic and static properties of soil. Nakamura [1] used the recorded microtremor data at a site to obtain the spectral amplification of a surface layer by evaluating the horizontal-to-vertical spectral ratio (HVSR). The horizontal-to-vertical spectral ratio has been validated by various authors by comparing simulations and earthquake recordings [2–6]. Various researchers [1,5,7] suggested that the maxima of the HVSR could be characteristic of the fundamental resonance frequency of a sedimentary cover and hence could be used to retrieve information regarding subsoil seismic layering [8–10]. The incident horizontal component of ground motion amplifies because of the presence of soft soil layers over the half space. The vertical component is equally influenced by site-effects but only at high

frequencies. The amplification effects of the vertical component are counterbalanced by the effect of refracting the ray path towards the vertical [11]. The peak frequency of HVSR is independent of source and time and the peak amplitude is only weakly sensitive [12,13]. Hence, HVSR is an approximate measure for estimating site amplification. Yaghmaei-Sabegh and Tsang [14,15] used artificial neural network on HVSR curve for determining the site class. However, Zhao et al. [16] and Di Alessandro et al. [17] used grouping of HVSR curves based on cumulative distribution of spectral shapes and defined a site classification index. As per Nakamura [18] and Herak [18], an HVSR curve is controlled by the body wave; however, as per Arai and Tokimatsu [8] and Lunedei and Albarello [19], surface waves play the major role. Bard [20] concluded that both models correctly interpret HVSR maxima as representative of the fundamental resonance frequency of the sedimentary layer. The fundamental resonant frequency can be obtained either by ambient noise measurement [21–23] or through an HVSR obtained from earthquake data [10,24].

Another key parameter in determining the dynamic properties of a soil and that is widely used in site classification is the average shear wave velocity up to 30 m in depth. Stewart et al. [25] found that for long-period earthquakes neither shear-wave velocity classification nor detailed surface geology can provide an optimal predictive scheme. Di Giacomo et al. [26] concluded that  $V_{S30}$  could also be misleading in the

\* Corresponding author at: Department of Civil Engineering, Indian Institute of Science, Bangalore 560012, India.

E-mail addresses: [anbazhagan2005@gmail.com](mailto:anbazhagan2005@gmail.com), [anbazhagan@iisc.ac.in](mailto:anbazhagan@iisc.ac.in) (P. Anbazhagan).

case of a shallow velocity inversion, i.e., to a depth of 19 m. Whereas Borchardt [27] stated that direct measurement of  $V_{S30}$  provides accurate characterization of a site for estimating the amplification factor and permits site classification unambiguously. Despite some criticism,  $V_{S30}$  is adopted as the main parameter for site classification in terms of seismic response by EuroCode8, the National Earthquake Hazard Reduction Program (NEHRP), the Electrical Power Research Institute (EPRI), and the American Society of Civil Engineers (ASCE). Researchers such as Abrahamson et al. [28] and others [29,30] have used  $V_{S30}$  as a descriptive variable for site effect in the Ground-Motion Prediction Equation (GMPE). Geophysical methods such as multi-channel analysis of surface waves and spectral analysis of surface waves are widely used for determining shear wave velocity to 30 m depth [31–33]. In India, various authors have used  $V_{S30}$  for site classification of different cities viz. Delhi [34], Guwahati [35] Dehradun [31], Bangalore [32], and Lucknow [36]. It can also be noted that  $V_{S30}$  is inadequate to estimate seismic amplification at a site as response from shallower depths also have a significant contribution [37,38].

In this study, HVSR has been used to determine the seismic site classification and its maxima to estimate the resonant frequency of seismic station sites in the Himalayan region. In total, 247 earthquake records from 167 stations were used, which had a moment magnitude ( $M_w$ ) varying from 2.3  $M_w$  to 7.8  $M_w$  and a Peak Ground Acceleration (PGA) value greater than 0.01 g. Based on the filtered and baseline-corrected ground motion, pseudo response spectra (5% damped) for both the horizontal and vertical components were obtained. The horizontal-to-vertical response spectral ratios (HVPSRs) were computed for the stations having more than one record available. The average of the HVSR was computed for all the stations. Based on HVSR, the peak frequency of individual stations was obtained and used to classify the stations according to the scheme of the Japan Road Association (JRA), 1980. Further, using the peak amplitude ( $A_{peak}$ ) and peak frequency ( $f_{peak}$ ) of HVSR,  $V_{S30}$  for various stations was determined using an empirical relationship developed by Ghofrani and Atkinson [11]. Because the results that were obtained using the two methods showed a great disparity, a new method was sought. A site classification index proposed by Ghasemi et al. [39], which is based on correlating the shape of HVSR curves of different site classes with the HVSR curve of the given station under question, was used. There are no standard curves for different site classes available for the Himalayan region. Hence, this has been resolved by using the existing HVSR curves of JRA [40] and Di Alessandro et al. [17] as both regions have similar seismotectonic characteristics. Additionally, method proposed by Phung et al. [41] is used for classifying seismic stations as rock and soil. A site classification is assigned to each station according to the results of all the methods, taking into consideration the available borehole data and surface geology. This study would be useful for the development of GMPE, determination of resonance conditions and amplification estimation due to soil, which are essential input for design of earthquake-resistant structures and infrastructure developments in the Himalayan region.

## 2. Study area and database

The Himalayan region, 2500 km in length, extends from Kashmir in the northwest to Arunachal Pradesh in the northeast and is one of the most seismically active regions in the world. The Indian plate converges northward at a rate of 50–65 mm/year [42] pushing against the Eurasian plate. As a result, there is a build-up of strain energy beneath the Earth's surface resulting in devastating earthquakes (1905 Kangra, 1934 Bihar–Nepal, 1950 Assam, 1988 Nepal, 1991 Uttarkashi, 1999 Chamoli, 2011 Sikkim, and 2015 Nepal earthquakes). The rapid drift of the thin Indian plate towards the Himalayan region in a northeastern direction is a cause of increased seismicity on the Indian subcontinent [43]. Based on historical earthquake data and the rupture extent of great earthquakes, various authors [44–47] have suggested that some segments under the Himalayan arc have not experienced a great

earthquake in the past 100 years. These are called seismic gaps. These gaps are the Kashmir gap that lies west of the 1905 Kangra earthquake rupture [44,45], the Central gap between the 1905 Kangra and 1934 Bihar–Nepal earthquakes [44] and the Assam gap region between the 1950 Assam and 1897 Shillong Plateau earthquake ruptures [48]. These regions have the potential to generate earthquakes soon [47]. Moreover, a study carried out by Hough and Bilham [49] estimating ground motion at hard sites from the large earthquakes of 1897 (Shillong), 1905 (Kangra), and 1934 (Nepal–Bihar) reflected the site effect in the Indo Gangetic Basin (IGB). As per Srinagesh et al. [49], there is a progressive thickening of the sedimentary basin from south to north, which varies from 1.2 km at Bilaspur to about 0.5 km beneath Hamirpur. As per Singh [50], sediment fill in the Ganges foreland basin is an asymmetrical wedge with a thickness of a few tens of meters in the south and ~ 4 km in the northernmost part. Boreholes in and around Kanpur reveal a sediment thickness of 500–600 m and a basement mostly comprising granitic rocks [51]. Similarly, as per the Nepal 2015 earthquake, most of the damage has been seen in the Kathmandu Valley, which is due to site amplification of seismic waves because it is a sedimentary basin. A similar site effect was seen in the Bhuj earthquake (2001); several multi-storied buildings in Ahmedabad, situated 300 km from the earthquake epicentre, collapsed. This was attributed to the presence of partially saturated silty sand deposits in the region [52]. Hence, as sediment thickness varies considerably in IGB, any earthquake in the Himalayan region may cause extensive destruction more than 500 km away due to site amplification. Even though seismic intensity and magnitude have remained similar over the years, increasing population density has augmented the risk associated with earthquakes and hence, it has emphasized the need for seismic study in this region [53]. Complete knowledge of the geology of this region would be helpful in the assessment of seismic hazards and the design of seismic-resistant structures and disaster mitigation.

The recorded earthquake ground motion data used in this study were obtained from the Program for Excellence in Strong Motion Studies (PESMOS), the Department of Earthquake Engineering, Indian Institute of Technology, Roorkee (IITR) and the Consortium of Organizations for Strong-Motion Observation Systems (COSMOS). The IITR is operating a network of 300 strong-motion seismographs along the Himalayan belt and in adjoining regions [54] for monitoring earthquakes. In total, 298 seismographs were installed by IITR in the states of Punjab, Haryana, Rajasthan, Uttarakhand, Uttar Pradesh, Sikkim, West Bengal, Arunachal Pradesh, Assam, Mizoram, Andaman, and Nicobar and Delhi. These seismic stations essentially consist of a sensor to record ground motion, a GPS for accurate time and location, and a data storage device. These stations are spaced every 40–50 km in plains and every 25–35 km in hilly regions. All the data obtained from PESMOS were baseline-corrected and low-pass-filtered before dissemination. Whereas in some of the records taken from COSMOS, the higher trigger level of the accelerographs caused some of the ground motion records to have a baseline error; such records could not be used for the present study. A selected number of acceleration time histories of 261 earthquake records from 167 stations were finally available for use. The database of earthquakes used in this study is shown in Fig. 1 by dividing the whole area into north-eastern India and the remaining Himalaya. Earthquake ground motions with moment magnitudes ranging from 2.3 to 7.8 and PGA > 0.01 g were used for the study. The data obtained were baseline-corrected and band-pass-filtered between 0.75 and 0.9 Hz and 25–27 Hz. The filtered and baseline-corrected database was further used in determining the pseudo response spectra (5% damping) for both the horizontal and vertical components of ground motion. Further, HVSR has been calculated for estimating its maxima which helps in determining the resonant frequency with respect to the station and earthquake used in this study. Ratios of pseudo-response spectra have been employed instead of Fourier response spectra, as they do not require additional smoothing [55] due to the single-degree-of-freedom system. The whole procedure of obtaining

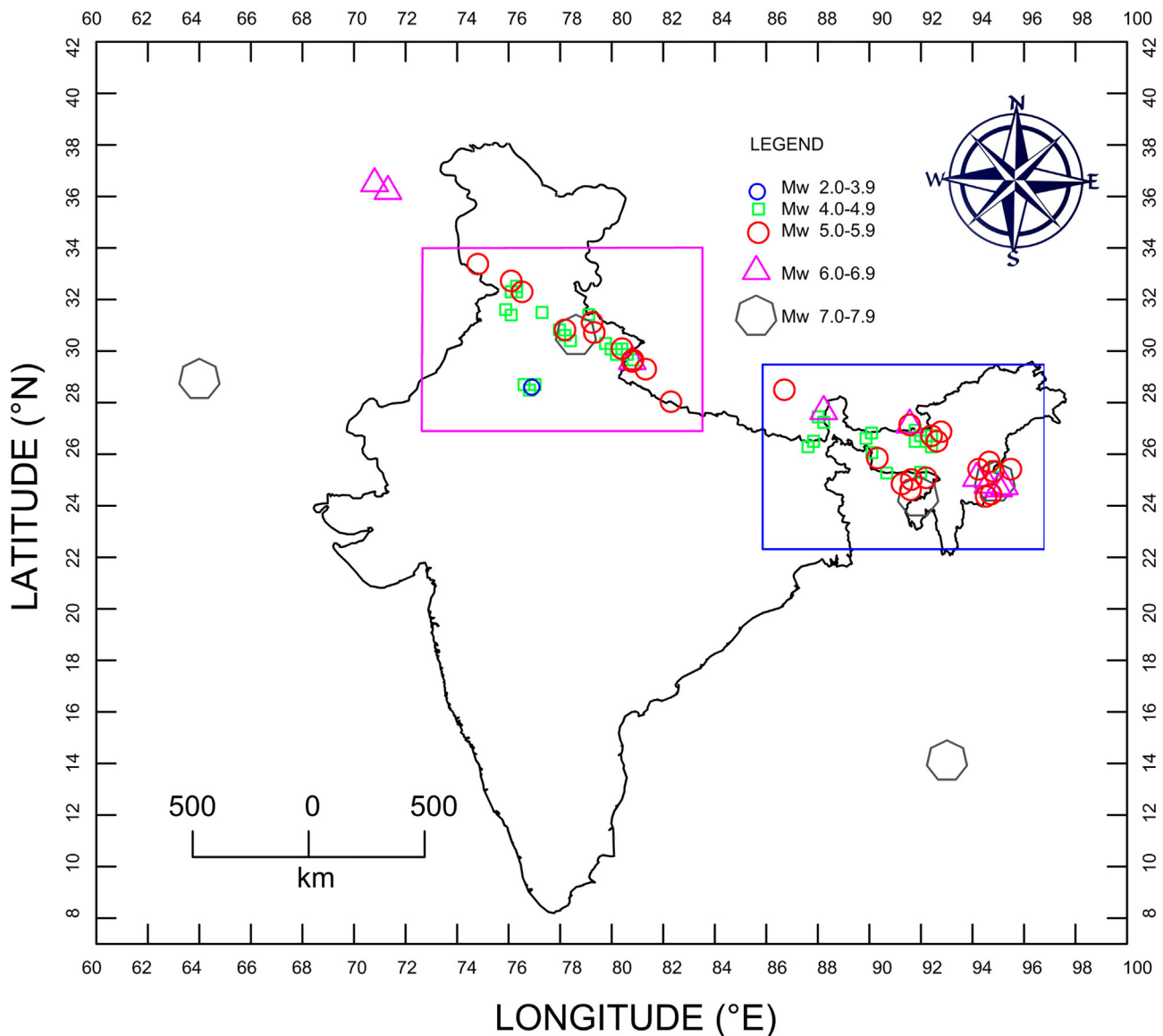


Fig. 1. Map showing the distribution of seismic events used for the study.

HVSR using orthogonal time history is given in Fig. 2. Fig. 2 shows the peak amplitude ( $A_{peak}$ ) and peak frequency ( $f_{peak}$ ) of HVSR which has been used for deriving  $V_{S30}$  as explained in the next section. Site classification according to NEHRP is based on  $V_{S30}$ . The developed HVSR has been further used to calculate  $V_{S30}$  and the seismic site classification of the 167 stations. Mittal et al. [56] has provided seismic site classifications of these station sites based on seismotectonics and a geological map of India. Both of these are insufficient to estimate the seismic response of a site with a complex ground response. Hence, in this study, an attempt has been made to classify these seismic station sites based on predominant frequency and shape of HVSR curves from the recorded data base obtained from each station.

### 3. Methodology

#### 3.1. Spectral ratio calculation

To encompass the regional site effects, HVSR has been used by various authors as previously explained. Theodulidis et al. [57] and Lermo and Chavez-Garcia [3] showed that HVSR is a simple but a stable indicator of site amplification. As per Atkinson and Cassidy [58],

characteristics of HVSR may indeed be largely accredited to the amplification of horizontal-component motions in the near-surface velocity gradient as compared to the theoretical amplification function. Thus, HVSR can be used as an approximate estimate of overall site effects and also in distinguishing between rock and soil conditions, especially in India, where such classification of seismic stations is not always available. The filtered time histories corresponding to different earthquakes (see Fig. 1) and different stations have been used in the determination of HVSR. The considered stations recorded a minimum of one earthquake and a maximum of twelve earthquakes. Only records having three components (two horizontal and one vertical) were used to compute the HVSR. The pseudo-response spectral accelerations (5% damped) of all three components (two horizontal and one vertical) of the acceleration time history of earthquake records were obtained at a time step of 0.02 s. Horizontal-to-vertical response spectral ratio has been calculated by dividing the geometric mean of the horizontal spectra by the smoothed amplitude spectrum of the vertical component as follows:

$$\log\left(\frac{H}{V}\right)_{ij} = \frac{\log H_1 + \log H_2}{2} - \log V, \tag{1}$$

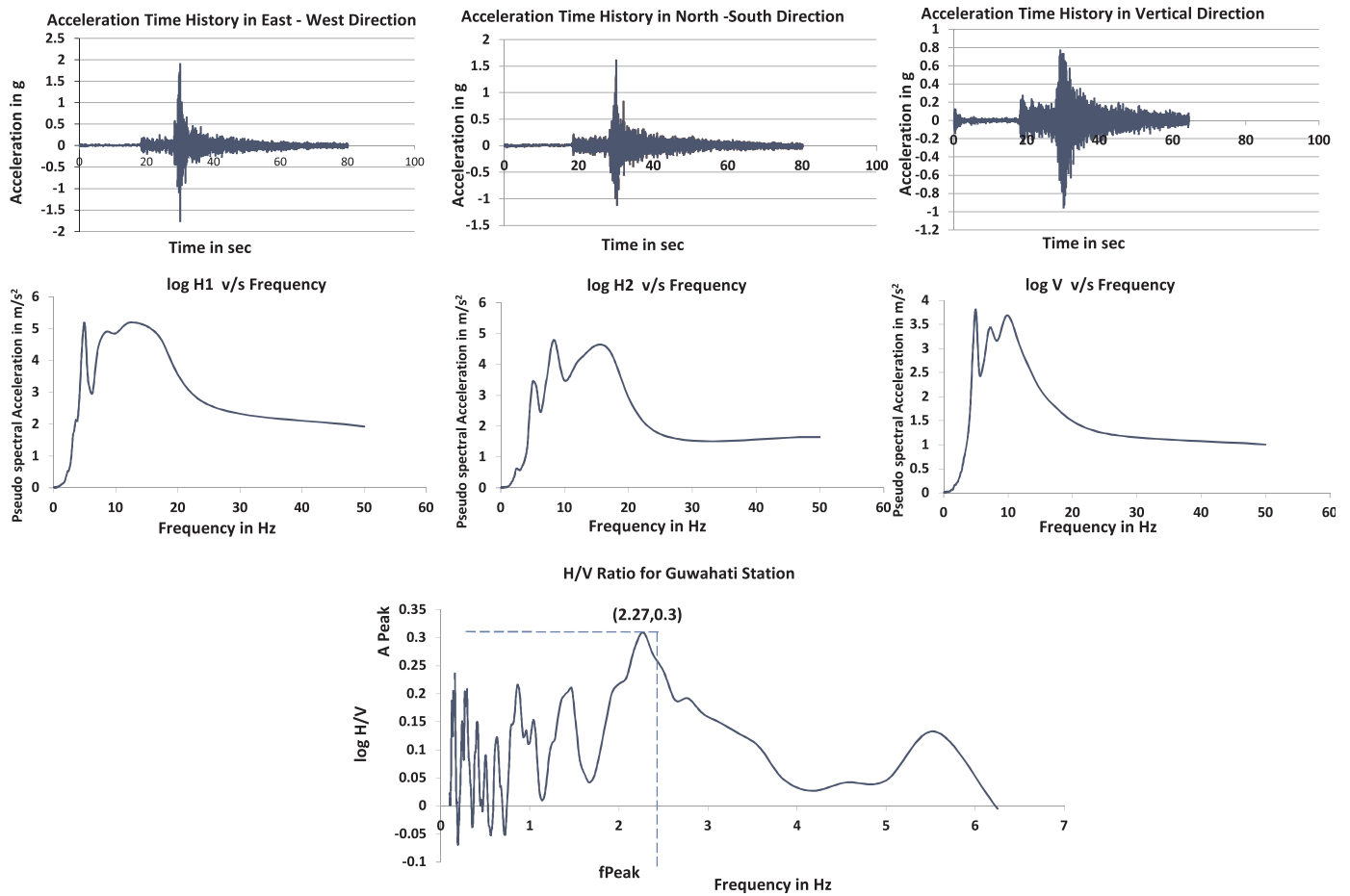


Fig. 2. Pseudo spectral accelerations are obtained from acceleration time histories and used to find H/V spectrum with  $f_{peak} = 2.27$  and  $A_{peak} = 0.3$ .

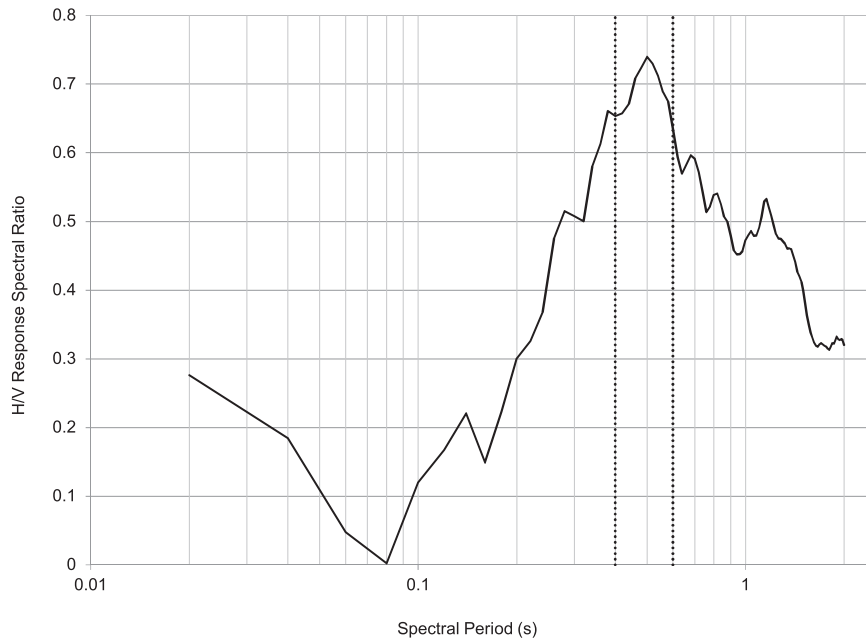


Fig. 3. Average H/V response spectral ratio for Dhanaulti station.

where  $H_1$  and  $H_2$  are the pseudo-response spectral acceleration (PSA, 5% damped) of the horizontal east-west, and north-south components, respectively, and V is the PSA corresponding to the vertical component at station  $i$  from earthquake event  $j$ . Further, HVSR at each station is

calculated as the mean of the  $\log\left(\frac{H}{V}\right)$  values, evaluated at frequencies in a range of 0.1–25 Hz at a frequency step of 0.02 Hz on a log scale as follows:

$$\log\left(\frac{H}{V}\right)_i = \frac{\sum_{j=1}^{N_i} \log\left(\frac{H}{V}\right)_{ij}}{N_i} \tag{2}$$

where  $N_i$  is the number of events recorded at the  $i^{th}$  station.

### 3.2. Site classification according to the predominant period

Kanai and Tanaka [59] were the first to propose a site classification based on predominant period. Zhao et al. [16] defined four site classes for Japanese strong-motion stations using predominant site period. This classification is also used in Japanese seismic design criteria for highway bridges by the JRA [40]. Fukushima et al. [60] also classified stations using predominant period obtained from average horizontal-to-vertical (H/V) ratios and used the scheme to derive GMPE's having lower standard deviations. The average HVSR curve for each station is computed. The frequency corresponding to the peak value of the HVSR curve is equivalent to the predominant frequency of the site (Nakamura, 1989). This is the natural period of the site and is used for identifying the site class by comparison to the JRA [40] recommended site-dependent period ranges. According to the JRA [40], sites were categorized as rock, hard soil, medium soil, and soft soil with natural periods of  $T < 0.2$  s,  $0.2 \leq T < 0.4$  s,  $0.4 \leq T < 0.6$  s, and  $T > 0.6$  s, respectively. The typical average HVSR curve at the Dhanaulti station is shown in Fig. 3. It shows a peak at 0.48 s. Hence, the Dhanaulti station is assigned as site class D. The geological profile and the topography were not considered in this system of classification. The recurring predominant period amongst the records in a station was used to determine the site class of that station. Stations with only single records were also classified. According to Luzi et al. [61], site classification based on single frequency value also gives good results. It was observed in this study that within a station, different earthquake records showed different peak periods. This is due to the variation in the frequency content of the different input motions used. Soft soils amplify low-frequency input motions more strongly than harder soils, and vice versa could be expected for high-frequency motions. At the Champawat station,  $f_{peak}$  values ranged from 0.22 Hz to 6.25 Hz. The  $f_{peak}$  from the averaged HVSR curve gave a peak frequency of 5.55 Hz (class A + B). Also, most records showed peaks more than 5 Hz (class A + B). Hence, it is preferable to have more than a single record to establish a station's site class based on predominant period. Fig. 4 shows a few of the H/V response spectral ratios observed at Champawat station. The dotted lines indicate ratios having  $f_{peak}$  values of approximately 5 Hz. The solid line is the average response spectral ratio for the Champawat station.

The double line shows an H/V ratio having a first predominant peak at 1.66 Hz and two secondary peaks at 3.33 Hz and 6.25 Hz. Another H/V ratio shown by the squared dotted line shows  $f_{peak}$  at 0.22 s, although we can see that the first peak is clearly at 5.55 Hz. The trends of the H/V ratios should be inspected individually and the  $f_{peak}$  values cannot be assigned as the maximum value observed. Also, the range of frequency over which the ratio is computed is to be predetermined for accurate results.

At some stations, multiple peaks were observed in the average HVSR curve, which gave misleading site classes. For example, at station Alipur, amplification peaks denoted site classes C and E with corresponding periods at  $T = 0.28$  s and  $T = 0.92$  s, as shown in Fig. 5. The larger is at 0.28 s. Later, using other methods, it was learned that the site class of the Alipur station is actually D; this will be discussed later in the paper. Hence, it is difficult to discern from this technique the exact site class in such cases. Furthermore, the comparison is done with different site classes assigned to these stations based on geological conditions by Kumar et al. [54].

When compared to the existing site classification of the COSMOS and PESMOS stations, 60 stations out of 167 stations showed disagreement. All the stations were considered for this result even though there were 27 and 47 stations with only single earthquake record under COSMOS and PESMOS, respectively. This could indicate the need for a revision of the site classification currently being used or that there could be an error in the method followed owing to the fact that it is based on only one single parameter indicative of site response. In order to gain further knowledge of site parameters, we tried using the relations derived for similar interplate regions for obtaining  $V_{S30}$  from HVSR curves.

### 3.3. $V_{S30}$ estimation using HVSR

Ghofrani and Atkinson [11] developed relationships between  $V_{S30}$  and the parameters of the H/V curve, namely,  $A_{peak}$  and  $f_{peak}$ . The method to obtain  $A_{peak}$  and  $f_{peak}$  is shown in Fig. 2. This relation was developed using data obtained from the Japanese database of the K-NET and KiK-NET stations of the National Research Institute for Earth Science Disaster Prevention. It was further found to be applicable to the NGA-West 2 database, which has earthquake records from all over the world, including China, Taiwan, Japan, Italy, and Southern and Northern California. The relations are the following:

$$\log(V_{S30}) = 2.80(\pm 0.02) + 0.16(\pm 0.02)\log(f_{peak}) - 0.50(\pm 0.03)\log(A_{peak}) \tag{3}$$

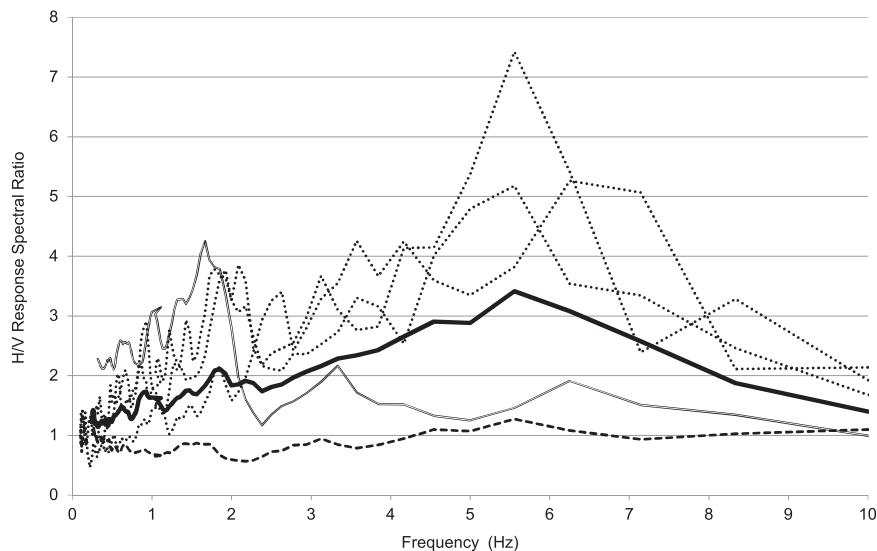


Fig. 4. H/V response spectral ratios observed at Champawat station.

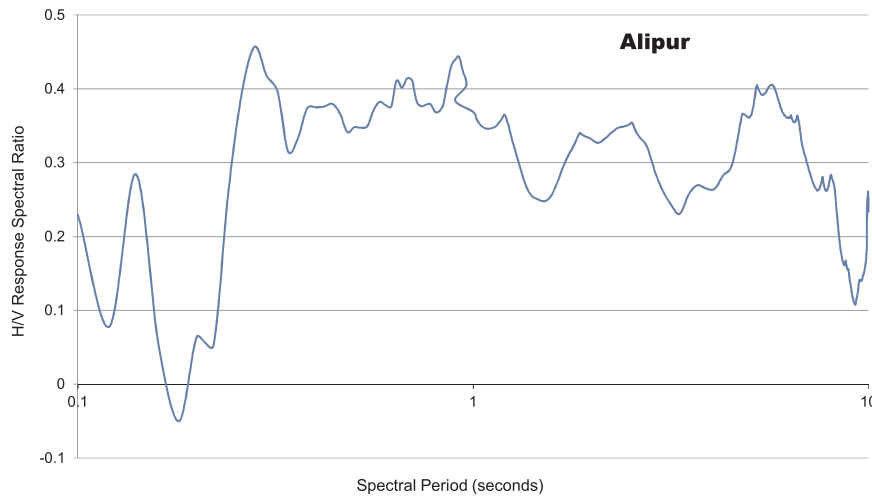


Fig. 5. Average H/V response spectral ratio for Alipur station.

$$\begin{aligned} \text{Log}(V_{s30}) = & 2.63(\pm 0.02) + 0.30(\pm 0.02)\text{log}(f_{peak}) \\ & - 0.47(\pm 0.03)\text{log}(A_{peak}) \end{aligned} \quad (4)$$

Eqs. (3) and (4) were developed using the NGA-West 2 and Japanese databases, respectively. The  $V_{s30}$  value calculated from Eq. (3) and Eq. (4) is within a factor of 1.41 (0.15 log units) and 1.38 (0.14 log units) respectively. Both equations were valid only for sites with  $f_{peak} > 1$ . The NGA-West 2 is a global database containing records from worldwide shallow crustal earthquakes in seismically active regions. The applicability of the two equations for the Indian subcontinent has been assessed. Because the Himalayan region has similar seismicity and seismotectonic features as those of NGA-West and Japan, these equations could be applicable to the present study area. The predicted  $V_{s30}$  value from Eqs. (3) and (4) has uncertainty as the developed equations do not have data from the Indian subcontinent. Because of the lack of estimated shear wave velocity profiles for seismic station, it is difficult to calculate these uncertainties. However, the final site class of seismic station is given based on different methods, which is explained further.

Hence, using HVSR, peak amplitude ( $A_{peak}$ ) and peak frequency ( $f_{peak}$ ) at each station was determined to calculate the shear wave velocity at 30 m depth ( $V_{s30}$ ) for each station. Hence, using both equations,  $V_{s30}$  at various sites was calculated and these stations were classified according to different sites as per the NEHRP building code. Site classes A, B, C, D and E are assigned to sites with  $V_{s30}$  values in the range of  $V_{s30} > 1500$  m/s,  $1500$  m/s  $> V_{s30} > 76$  m/s,  $760$  m/s  $> V_{s30} > 360$  m/s,  $360$  m/s  $> V_{s30} > 180$  m/s and  $V_{s30} < 180$  m/s, respectively. The results yielded mostly site classes D and C for 92 and 70 stations, respectively. These classes were checked with the predominant-period-based classification determined previously.

Only one station was classified A+B and five stations were identified as class E. Fig. 6(b) and Fig. 6(c) show the estimated site classes from  $f_{peak}$  and  $V_{s30}$  values, respectively. It shows the number of stations assigned for each site class. The method fails to predict A+B and E classes. For example, at the Baigao station, where the peak frequency is approximately 8.33 Hz from all the records, clearly indicates a site class of A+B, yet the  $V_{s30}$  values from the equation gave much lower values corresponding to the D and C classes with maximum value of  $V_{s30}$  at 374 m/s. Similarly, for stations Naogaon and Barpeta, the  $V_{s30}$  values ranged between 275 and 331 m/s (class D), which, according to  $f_{peak}$  values, had clearly shown site class E in all its records.

Most of the class C stations were predicted. A+B stations were assigned to a nearby site class of C. Within a station, the site classes were, however, mostly constant. Hence, this method can be used to yield approximate results. However, an additional method more suitable to the region was sought.

### 3.4. Site classification according to the shape of HVSR curve

The shape of an HVSR curve is characteristic of each site class with the peak falling under a certain range of frequency and amplitude. This can be used to identify the site class of each seismic station. Normalized acceleration spectra have been used for shape-based response spectral classification [62]. Zhao et al. [16] introduced a grouping of HVSR curves based on the cumulative distribution of spectral shapes and defined a site classification index. Ghasemi et al. [39] adopted a similar method for Iranian seismic stations. A site classification index given by Spearman's correlation coefficient has been used. The present study uses this method. The site classification index is defined as follows:

$$SI_k = 1 - 6 \sum \frac{d_i^2}{n(n^2-1)}, \quad (5)$$

where  $d_i$  is the difference in ranks of  $x_k$  and  $y$ ;  $x_k$  is the mean of the HVSR curve for the  $k^{\text{th}}$  class,  $y$  is the mean HVSR curve for the station under consideration, and  $n$  is the total number of periods. Spearman's correlation is a nonparametric measure of the statistical dependence between two variables. Its value ranges from  $-1$  to  $+1$ ; a positive correlation shows an increasing monotonic trend between the variables  $x_k$  and  $y$ . A negative value shows a decreasing correlation between the variables. A zero value means the trend between the two variables neither increases nor decreases or that the increasing and decreasing trends are equal so as to neutralize the net correlation outcome.

As the actual site classes of the strong motion stations are not known, the averaged HVSR curves of the stations have been correlated with HVSR curves given for K-net stations by Zhao et al. [16]. It consisted of HVSR curves for four site classes SC-I, SC-II, SC-III, and SC-IV that come under the NEHRP site class definitions of A+B, C, D, and E, respectively. Here, class A+B indicates  $V_{s30} > 600$  m/s. Site classes C, D, and E belonged to the  $V_{s30}$  ranges of  $300$  m/s  $< V_{s30} \leq 600$  m/s,  $200$  m/s  $< V_{s30} \leq 300$  m/s, and  $V_{s30} < 200$  m/s, respectively. Hence, HVSR curves were digitized and values of the H/V ratios corresponding to various spectral periods were obtained. The obtained curve had a period range between 0.06 and 3.26 s. In order to correlate the digitized curve with that of the unknown HVSR curve, it is necessary to obtain the values of the H/V ratios during the same spectral periods. Many times, this was approximated to the nearest spectral period with a maximum error of  $\pm 0.009$  s. These values of the HVSR curves were used for correlation with the averaged HVSR curves of each station. The site class which repeated the most within a station was assigned to it. Fig. 6(d) shows the site classes obtained using this method. Classes obtained were in near agreement to the existing classification at most stations. A few stations have a stark contrast with earlier classification

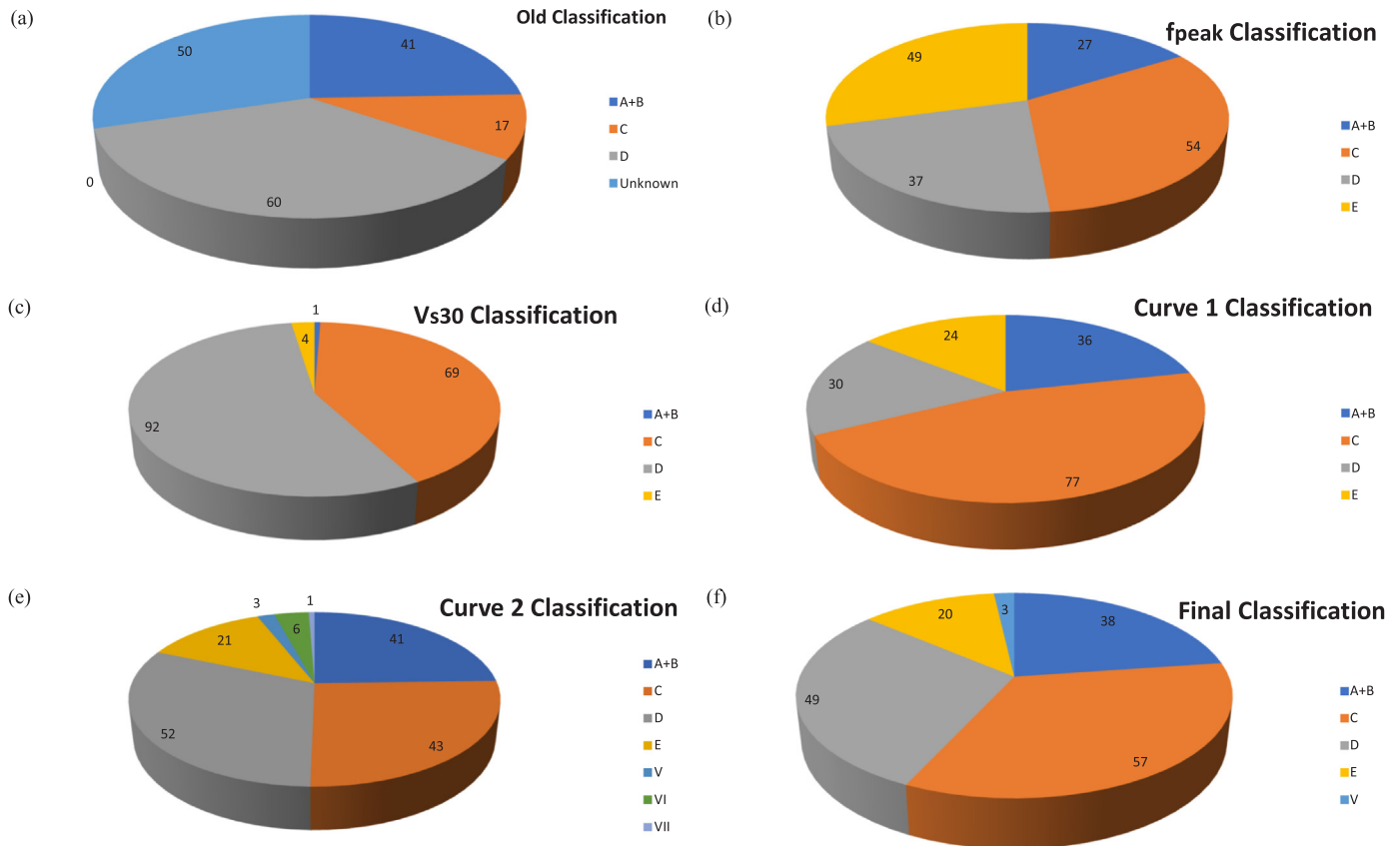


Fig. 6. Number of stations coming under each site class using different classification methods: (a) Existing Classification, (b) Predominant Period based (c)  $V_{s30}$  classification, (d) from Curve 1, (e) from Curve 2.

even when the numbers of the earthquake records at these stations were around 4–8 in number. It was found that most of these stations were classified as site class C. Many stations also came under site class E, suggesting soft soil with  $V_{s30} < 200$  m/s. This is an unfavourable site condition for a seismic station. High values of seismic noise and a reduction in maximum possible gain will be observed at these stations. To validate the findings, we approached a broader site classification.

Di Alessandro et al. [17] gave a site classification scheme for Italian stations based on the predominant period obtained from the H/V spectral ratios. It consists of the four classes given by Zhao et al. [16] and additional three classes. Class V was assigned for stations with a flat average H/V response spectral ratio ( $< 2$ ) with no significant peak. It represented generic rock sites. Class VI was assigned to generic soil sites whose H/V ratios showed broad amplification or multiple peaks at periods greater than 0.2 s. In the case that there were multiple peaks before and after 0.2 s, it was termed unclassifiable (Class VII). The seven HVSr graphs were digitized in the period range of 0.06–2 s with an error of  $\pm 0.008$  s. Correlation with average HVSr curves of stations was completed using Spearman's rank-based correlation which has a range from  $-1$  to  $+1$ . Those records which gave negative values of correlation were not used to compute the average value of the HVSr. Fig. 6(e) shows the total number of different site classes obtained using this method. It was found that some of the stations were site class E. This was also corroborated by the predominant period values of  $< 1.66$  s at these stations. The results were in agreement with the previously obtained site classes. It was also observed that the variation in site classes within a station was not more than one unlike that of the previous methods. Some stations also indicated site classes corresponding to generic rock (class VI) and generic soil (class VII). Station Jaffarpur came under site class VII (unclassifiable) as multiple peaks were observed before and after  $T = 0.2$  s. This can also be due to unavailability of sufficient records. Only three records were available and

numerous negative correlation coefficients were observed. The results obtained using all four methods are given in Table 1. The site classes for curve 1 and curve 2 do not always correspond to the site classes which obtained the highest correlation coefficient. Sometimes the actual site class may be that with a slightly lower value correlation coefficient but it is the most recurrent amongst all the records, hence it is assigned.

### 3.5. Site classification according to PSA shape

Phung et al. [41] considered the shape of the 5% damping pseudo spectral acceleration (PSA) of horizontal ground components normalized with respective peak ground acceleration (PGA) value for site classification. This technique is used for classifying site either as Rock (R) or Soil (S). The following is the procedure described by Phung et al. [41] for site classification

1. The 5% damped pseudo-acceleration spectra of two horizontal components of ground motions are computed. Further, the smoothed spectra are normalized by dividing them by the PGA.
2. For stations with closest distance ( $d_{rup}$ ) is more than 40 km i.e.  $d_{rup} > 40$  km, the predominant period ( $T_g$ ) can be used as a discriminant to distinguish between rock and soil sites. The site having  $T_g \geq 0.6$  s is classified as soil, whereas, the site is classified as rock if  $T_g < 0.6$  s.
3. For stations with  $d_{rup} \leq 40$ ,  $PSA(2.5)/PGA$  can be used as a discriminant for site classification. If  $PSA(2.5)/PGA \geq 0.7$ , then the site is classified as soil, while if  $PSA_{PGA}^{2.5} > 0.7$ , then the site is classified as rock.

Note: if the spectrum has a plateau extending over a period range that exceeds 0.6 s, it is classified as soil even if the period at which the maximum amplitude occurs is actually below 0.6 s.

**Table 1**  
Final site class according to different methods.

Sl. no	Station	Lat (° N)	Long (° E)	Site class based on					Final
				f peak	VS30	Curve 1	Curve 2	Phung et al. (2006)	
1	Haflong	25.17	93.02	A + B	D	A + B	5	S	5
2	Bhatwari	30.8	78.22	E	D	E	5	S	5
3	Umrongso	25.51	92.63	D	D	A + B	5	S	5
4	IMD	28.68	77.21	A + B	C	C	C	S	C
5	IGNOU	28.49	77.2	C	C	C	A + B	S	C
6	CRRI	29.02	77.05	A + B	B	A + B	A + B	R	A + B
7	Champawat	29.33	80.09	A + B	C	A + B	A + B	R	A + B
8	Jowai	25.44	92.2	A + B	C	A + B	A + B	R	A + B
9	Pithoragarh	29.58	80.21	A + B	D	A + B	A + B	R	A + B
10	Rudraprayag	30.29	78.98	A + B	C	A + B	A + B	R	A + B
11	Baigao	25.41	92.86	A + B	D	A + B	A + B	R	A + B
12	Panimur	25.66	92.8	A + B	D	A + B	A + B	R	A + B
13	Saitsama	25.72	92.39	C	D	A + B	A + B	R	A + B
14	Shillong	25.57	91.89	A + B	C	A + B	A + B	R	A + B
15	Ummulong	25.52	92.16	A + B	C	A + B	A + B	R	A + B
16	Cherapunji	25.3	91.7	A + B	C	C	A + B	R	A + B
17	Harengajao	25.11	92.86	D	D	A + B	A + B	R	A + B
18	Khlieriat	25.36	92.37	C	D	A + B	C	S	C
19	Mawphalang	25.46	91.77	A + B	D	A + B	A + B	R	A + B
20	Andc	28.54	77.26	A + B	C	A + B	A + B	R	A + B
21	Uttarkashi	30.73	78.44	A + B	C	A + B	A + B	R	A + B
22	Hamirpur	31.69	76.52	C	D	A + B	A + B	R	A + B
23	Recong Peo	31.54	78.27	C	C	A + B	A + B	R	A + B
24	JNU	28.54	77.17	A + B	D	A + B	A + B	S	A + B
25	Jubbal	31.11	77.66	A + B	C	A + B	A + B	R	A + B
26	Djb	28.65	77.19	A + B	C	A + B	A + B	S	A + B
27	Bandlakhas	32.13	76.54	C	D	A + B	A + B	S	C
28	Baroh	31.99	76.31	D	D	C	A + B	S	D
29	Laisong	25.2	93.31	A + B	C	C	A + B	R	A + B
30	Maibang	25.31	93.14	A + B	C	A + B	A + B	R	A + B
31	Karnprayag	30.25	79.23	C	D	D	A + B	R	A + B
32	Srinagar	30.22	78.77	A + B	C	D	A + B	R	A + B
33	Kosani	29.68	79.72	A + B	C	A + B	A + B	R	A + B
34	Rakh	32.466	76.233	A + B	C	A + B	A + B	R	A + B
35	Landsdown	29.84	78.68	D	C	A + B	A + B	R	A + B
36	Chinyalisaur	30.55	78.33	C	D	A + B	A + B	R	A + B
37	Bhawarna	32.05	76.5	E	D	C	A + B	R	A + B
38	Ukmath	30.5	79.1	E	D	A + B	A + B	R	A + B
39	Purola	30.87	78.08	E	D	A + B	A + B	R	A + B
40	Keylong	32.56	77.01	E	C	A + B	A + B	R	A + B
41	Munsiari	30.07	80.24	E	C	A + B	A + B	R	A + B
42	Kapkot	29.94	79.9	C	D	C	C	R	C
43	Kashmiri Gate	28.665	77.232	C	D	C	A + B	S	C
44	Mayur Vihar	28.6	77.3	C	C	C	6	S	C
45	Kashipur	29.21	78.96	C	D	C	C	S	C
46	Alwar	27.57	76.59	C	D	C	D	S	C
47	Darjelling	27.05	88.26	C	C	D	D	R	C
48	Rampur	31.45	77.63	C	D	C	D	S	C
49	Sonipat	29	77	C	C	C	D	S	C
50	Joshimat	30.57	79.58	C	C	C	C	R	C
51	Dlu	28.69	77.21	E	D	C	C	R	C
52	Chakrata	30.69	77.9	C	C	C	D	R	C
53	Dee	28.8	77.12	E	D	D	E	S	C
54	Bageshwar	29.83	79.77	C	D	C	C	S	C
55	Barkot	30.81	78.21	C	D	C	D	S	C
56	Tehri	30.37	78.43	E	C	C	D	S	C
57	Rishikesh	30.12	78.28	C	D	D	C	S	C
58	Nongkhlaw	25.69	91.64	C	D	C	D	S	C
59	Umsning	25.74	91.89	C	C	C	C	R	C
60	Dauki	25.19	92.03	C	C	C	C	R	C
61	Nonpoh	25.92	91.88	C	C	D	C	R	C
62	Gunjung	25.32	93.01	C	D	C	C	R	C
63	Jellalpur	25	92.46	C	C	A + B	C	R	C
64	Jhirghat	24.81	93.11	C	C	C	C	S	C
65	Nathpa	31.55	77.92	C	C	C	C	S	C
66	Pauri	30.15	78.78	C	C	C	C	S	C
67	Tinsukia	27.5	95.33	C	C	C	C	S	C
68	Kullu	31.96	77.11	C	C	C	D	S	C
69	Dharamshala	32.21	76.32	C	C	C	C	S	C
70	Golaghat	26.51	93.97	E	D	C	D	S	C
71	Indraprastha University	28.66	77.23	C	C	C	C	S	C
72	Jamia	28.53	77.27	A + B	D	D	D	S	D

(continued on next page)

Table 1 (continued)

Sl. no	Station	Lat (° N)	Long (° E)	Site class based on					Final
				f peak	VS30	Curve 1	Curve 2	Phung et al. (2006)	
73	Dehra	31.88	76.22	D	C	C	A+B	R	C
74	Jawali	32.14	76.01	C	C	C	6	S	C
75	Kangra	32.1	76.26	C	D	C	D	R	C
76	Nagrota Bagwan	32.1	76.38	C	D	C	C	R	C
77	Shahpur	32.21	76.19	C	D	C	C	S	C
78	Ghansiali	30.42	78.65	C	C	C	C	S	C
79	Patti	29.41	79.93	C	C	C	C	S	C
80	Sundernagar	31.52	76.88	C	C	A+B	D	S	C
81	Bahadurgarh	26.26	87.83	E	D	C	C	S	C
82	Nongstoin	25.52	91.26	C	C	D	C	R	C
83	Pynursula	25.31	91.91	A+B	C	C	C	R	C
84	Hajadisa	25.38	93.3	C	C	C	A+B	R	C
85	Hojai	26	92.86	C	C	D	C	S	C
86	Gangtok	27.35	88.63	C	C	C	C	S	C
87	Koteshwar	30.23	78.57	C	C	C	C	S	C
88	Koti	30.58	77.78	D	C	C	A+B	S	C
89	Kasauli	30.9	76.96	C	C	C	C	S	C
90	Karimganj	24.87	92.35	D	D	C	C	S	C
91	Lodhi Road	28.583	77.217	E	D	C	C	S	C
92	Didihat	29.77	80.3	E	D	C	C	S	C
93	Chamba	32.55	76.13	D	C	C	C	R	C
94	Bokajan	26.02	93.77	E	D	C	C	R	C
95	Hatikali	25.65	93.11	E	C	C	C	S	C
96	Almora	29.58	79.65	D	C	C	C	S	C
97	Gopeshwar	30.4	79.33	D	D	C	C	S	C
98	Sihunta	32.3	76.09	D	C	C	C	S	C
99	Dibrugarh	27.47	94.91	E	D	D	D	S	D
100	Tejpur	26.62	92.8	D	D	C	D	S	D
101	North Lakhimpur	27.24	94.11	D	D	C	D	S	D
102	Alipur	28.8	77.14	D	C	D	D	S	D
103	Palampur	32.11	76.54	E	D	C	D	R	D
104	Darchula	29.85	80.55	D	C	D	D	S	D
105	Dehradun	30.32	78.04	C	D	D	D	S	D
106	Tanakpur	29.07	80.11	A+B	C	D	C	R	D
107	Silchar	24.83	92.8	D	D	D	D	S	D
108	Berlongfer	25.77	93.25	D	D	C	D	S	D
109	Doloo	24.92	92.79	D	C	D	D	S	D
110	Jaffarpur	28.59	76.91	C	D	D	7	S	D
111	Baithalangso	25.97	92.6	A+B	C	D	D	R	D
112	Kalain	24.98	92.58	C	C	D	C	S	D
113	Katakhal	24.82	92.62	E	C	E	D	S	D
114	Noida	28.51	77.48	D	D	C	6/D	S	D
115	Zakir Hussain	28.64	77.23	D	D	D	D	S	D
116	Rohtak	28.9	76.59	E	C	C	D	S	D
117	Anandpur Sahib	31.24	76.49	C	D	D	D	S	D
118	Mandi	31.71	76.93	D	D	D	D	R	D
119	Mangaldai	26.44	92.03	D	D	D	D	S	D
120	Bilaspur	31.34	76.76	E	D	D	E	S	D
121	Tura	25.51	90.22	D	D	C	D	S	D
122	Guwahati	26.19	91.75	D	C	C	D	S	D
123	Raja Garden	28.66	77.12	E	D	D	D	S	D
124	Baraut	29.1	77.26	E	D	E	D	S	D
125	Araria	26.13	87.47	C	D	D	D	S	D
126	Udham Singh Nagar	29	79.4	D	D	C	D	S	D
127	Saluni	32.7	76.06	C	D	D	6/ D	S	D
128	Sonipat	29	77	C	C	D	D	S	D
129	Dasua	31.81	75.66	D	D	C	D	S	D
130	Dhanaulti	30.43	78.24	D	D	C	D	S	D
131	Khatima	28.92	79.97	D	D	C	D	S	D
132	Hailakandi	24.68	92.56	E	D	D	D	S	D
133	Una	31.47	76.26	E	D	E	6/D	S	D
134	Amb	31.69	76.12	E	E	D	D	S	D
135	Mukerian	31.95	75.61	E	E	C	D	S	D
136	Nawanshahar	31.12	76.12	E	E	D	D	S	D
137	Roorkee	29.86	77.89	E	D	C	D	S	D
138	Bamungao	25.89	93.01	E	C	C	6/D	S	D
139	Diphu	25.84	93.44	D	D	C	D	S	D
140	Jammu	32.73	74.87	D	D	C	D	S	D
141	Morigaon	26.25	92.34	D	D	C	D	S	D
142	Vikas Nagar	30.45	77.75	D	D	C	C	S	D
143	Gurdaspur	32.04	75.41	D	D	C	D	S	D
144	Siliguri	26.71	88.43	D	D	C	D	S	D
145	Jorhat	26.76	94.21	D	D	C	D	S	D

(continued on next page)

Table 1 (continued)

Sl. no	Station	Lat (° N)	Long (° E)	Site class based on					Final
				f peak	VS30	Curve 1	Curve 2	Phung et al. (2006)	
146	Sibsagar	26.99	94.63	D	D	C	C	S	D
147	Garsain	30.05	79.29	D	C	D	E	S	D
148	Dhubri	26.02	90	E	E	E	D	S	E
149	Barpeta	26.33	91.01	E	D	E	E	S	E
150	Garh Shankar	31.23	76.13	E	D	E	E	S	E
151	Kapurtala	31.38	75.38	E	D	E	E	S	E
152	Nakodar	31.12	75.49	E	D	E	E	S	E
153	Amritsar	31.64	74.86	E	D	E	E	S	E
154	Ballabgarh	28.34	77.32	E	D	E	E	S	E
155	Gurgaon	28.45	77.03	E	D	C	E	S	E
156	Palwal	28.13	77.33	E	D	E	E	S	E
157	Rewari	28.18	76.61	E	D	E	E	S	E
158	Bongaigaon	26.47	90.56	E	D	E	E	S	E
159	Port Blair	11.66	92.74	E	C	E	E	S	E
160	Kokhrajhar	26.4	90.26	E	C	E	E	S	E
161	Boko	25.98	91.23	E	D	E	E	S	E
162	Cooch Vihar	26.32	89.44	E	D	E	E	S	E
163	Kishanganj	26.1	87.95	E	D	E	E	S	E
164	Raxaul	26.98	84.84	E	E	E	E	S	E
165	Goalpara	26.16	90.63	E	D	E	E	S	E
166	Chamoli	30.41	79.32	E	D	E	D	S	E
167	Naogaon	26.35	92.69	E	D	E	E	S	E

Considering the criteria given by Phung et al. [41], all 167 stations have been classified. Out of 167, 114 stations are classified as soil and 53 as rock. Detail of the site classification is given as Table 1.

3.6. Final site class

A final site class was assigned to each station after comparing the results obtained using each technique. The most recurrent class obtained from the predominant period  $V_{s30}$  method as well as from rank-based correlations for all H/V ratios at a station was assigned as the final site class. All the stations were assigned site classes manually. Final site class is shown in Table 1. The pie charts in Fig. 6 indicate how the number of stations in each site class changed according to each method. The initial and final set of station site classes shows a huge variation. The least error is obtained from method four, namely, that where the site class was obtained through rank-based correlation with the second curve of Di Alessandro et al. [17]. However, this method could not predict the C and D classes very accurately. Predominant-period-based classification is also good in predicting the site class, with an equal amount of error throughout all site classes. Finally, the site classes of all stations, irrespective of the number of earthquake records, could be identified. For each site class, typical HVSR curves were drawn showing the maximum values of amplification and corresponding peak frequencies. The average HVSR response spectrum for each site class with the respective standard deviation is shown in Fig. 7. The curves fall within the period ranges as defined by the JRA [40]. The maximum

standard deviation is approximately 0.3, which is low compared to previous studies of Zhao et al., [16] and Di Alessandro et al. [17]. The maximum standard deviations for site classes A + B, C, D, and E are 0.2054, 0.3082, 0.1718, and 0.296 respectively. The differences between average HVSR curves for the different site classes are statistically significant except at  $T = 5.18, 3.22,$  and  $7.26$  s (for A + B and D sites),  $T = 0.26$  and  $2.04$  s (A + B and E sites), and  $T = 0.32, 0.64,$  and  $1.02$  s (D and E classes).

4. Validation through a regional site class study-Delhi region

Final site class assignments based on this study are further verified with available in-situ data. Delhi, the national capital of India, falls under seismic zones IV and V according to the Geological Survey of India. It confronts a substantial seismic threat due to the complex local tectonics and the seismically active Himalayas. Geological mapping and remote-sensing studies indicate the presence of many fault patterns. It is bound by several dominant geological features such as the Himalayan Main Boundary Thrust and the Main Central Thrust. It has the Delhi–Haridwar Ridge, the Delhi–Lahore Ridge, the Aravalli–Delhi fold axes, the Sohna Fault, the Mathura Fault, the Rajasthan Great Boundary Fault and the Moradabad Fault in addition to several other minor lineaments. The seismicity is mainly attributed to the Delhi–Haridwar Ridge, which has a northeast-southwest trend. The terrain is generally flat with the exception of a low north-northeast/south-southwest drifting ridge as the focal segment of the area. Iyenger and Ghosh [63]

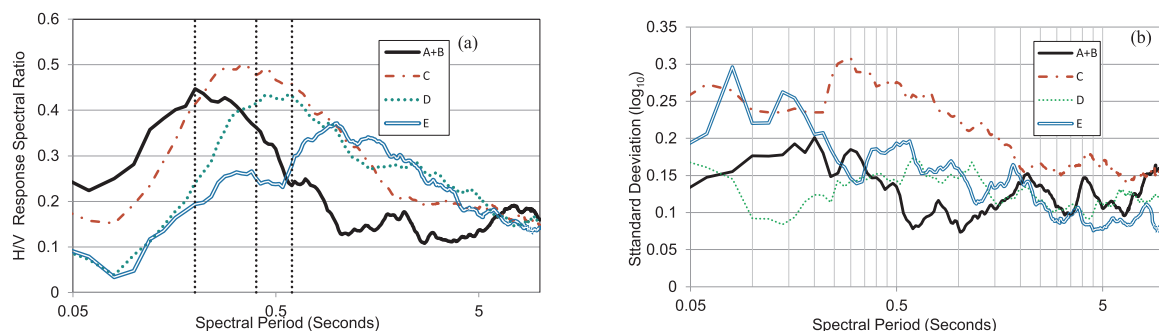


Fig. 7. Average HVSR curves for site classes A + B, C, D and E along with standard deviations.

described the lithology of Delhi and highlighted the presence of many paleochannels along the alignment of the River Yamuna. A major part of the Delhi belongs to flat alluvium and having variable bedrock depth. The major part of the Delhi region is covered by deep layers consist of alternative beds of silty sand and medium to low compressibility clays.

Number of studies have been carried out in the Delhi region related to site amplification. These studies are based on (1) using Microtremors [64], (2) recorded earthquake data [56,65,66], (3) standard penetration tests [63], and (4) numerical modelling of wave propagation (e.g., [67]). Pandey et al. [68] performed site characterization of strong-motion recording stations of the Delhi region using joint inversion of phase velocity dispersion curves and H/V curves. They conducted field testing at 19 strong-motion instrumentation sites. The site characteristics assessed were determined using joint inversion of multichannel analysis of surface waves and HVSR from ambient noise results simultaneously to estimate the shear-wave velocity profiles. The benefit of using this method is that it provides site characteristics assessed through the shear-wave velocity profiles down to much deeper soil strata. The results obtained were further validated using ground response analysis from the recorded ground motions.

The final shear-wave velocity profiles were compared to the site class values obtained in this study at 10 strong-motion stations in the Delhi region. Pandey et al. [68] has classified the 19 seismic stations at the Delhi region using joint inversion of HVSR and MASW. The stations classified in this study matched well with the study carried out by Pandey et al. [68]. For example, the site classification of the IMD and INGNOU sites as per the MASW test conducted by Pandey et al. [68] is C. IMD and INGNOU stations lied over silty sand and clay over Kankar as per Geological survey of India. As per Pandey et al. [68], shear wave velocity of more than 700 m/s is observed after 60 m depth. Silty sand is present till 20 m depth in around IMB and INGNOU stations [63]. Additionally, the final site classification of Delhi seismic stations along with geological classification [54] is given as Table 2 According to the site classification methodology used in this study, the site class of both the stations is also C. This further validates the utility and accuracy of the results and techniques employed.

### 5. Comparison of topography-based classification and spectral analyses

Topography is an important parameter which determines the surface properties at a site. It gives an indication of grain size. The steeper the slope, the harder the material and the higher the shear-wave velocity. Geological maps can be employed to obtain topographic slopes. Correlations between topographic gradient and  $V_{s30}$  were developed by Wald et al. [69]. Data has been made available by the Geological Survey of India (NSDI, nsdiindia.gov.in) in the form of geological maps. Nath et al. [70] used these correlations between  $V_{s30}$  and topographic

**Table 2**  
Seismic site classification of delhi stations along with geology and soil type.

S. no.	Station name	Classification		
		Pandey et al. [68]	Present Study	Soil type
1.	Jaffarpur	D	D	Clay with Kankar
2.	Raja Garden	D	D	
3.	Jamia	D	D	Quartzite with Schist
4.	JNU	D	A + B	Band
5.	Alipur	D	D	
6.	Delhi Jal Board	C	A + B	
7.	Kashmere Gate	D	C	Silty Sand with clay
8.	Zakir Hussein College	D	D	over Kankar
9.	IMD	C	C	
10.	INGNOU	C	C	

gradient for site characterizations of different regions in India. The site classes of the stations in the regions of Guwahati, Dehradun, and Delhi were obtained from the maps. Location of the Dehradun station was plotted on the corresponding maps. It presents its site class as D, which was as predicted by the final results of this study. Interestingly, it was found that except for the predominant-period-based classification which gave a site class of C, all the other methods identified the correct site class.

For station Guwahati, the position of the strong motion station was plotted. It indicated a site on the border of site classes C and D. The same result can also be observed from Table 1, wherein both site classes have been predicted equally. The maps for the Delhi region showed a site class C and higher near the quartzite region to the south. Most stations came under site class D. Stations could not be successfully matched owing to the lack of resolution in the map and an inability to locate stations accurately.

Nath et al. [70] appraises a topographic-gradient approach for site classification that employs correlations between 30 m column time-averaged shear-wave velocity and topographic gradients. They used the approach proposed by Wald and Allen [69] that correlates  $V_{s30}$  and topographical slopes for several cities across India. Classification of seismic stations broadly on a topographical level may not be significant, as the data from these recording stations need to be used in further studies. For example, based on the topographic gradient approach proposed by Nath et al. [70], the site class of Uttarkashi comes under “C” but the station is on rocky terrain; hence, classifying it as a site class “C” is not significant. Even considering Phung et al. [41], it is classified as rock site. Similarly, as per Nath et al. [70], the Sonipat station can be classified as site class “C,” but it lies in the Indus Basin and has deep silty strata, and therefore, classifying it as “C” is not significant. The same observations have been seen for the Delhi region, as per MASW conducted by Pandey et al. [68] presenting the site class at Jamia station as D. Using a topographic map by Nath et al. [70], it has classified it as site class C, however, using HVSR, it is classified as site class D. This shows that identification of site classes using a topographic map cannot be that effective. Moreover, it can be noted that topography along the Himalayan region is undulating and that an effect can be seen in different site classes for different stations in the region. Hence, instead of broad classification, regionally based classification of seismic stations need to be evaluated. Nath et al. [70] also used three empirical methods for site characterization of strong-motion stations in the Himalayan region using earthquake records, namely, HVSR, RSS, and HVRSR. A set of 65 stations were identified and found to correspond to the present study. At 52 stations, the site classes were agreeable to the present study. In some cases, wherein the numbers of records studied were few, site characterization was nearly predicted as the adjacent class; overall, the comparison yielded satisfactory results.

### 6. Discussions and conclusions

The Himalayan region is one of the most seismically active regions of the world. The fault rupture mechanisms are complex and vary across the region. India has deployed a set of 300 strong ground-motion stations to record earthquakes in this region. Site characteristic information is unavailable for the stations due to the high cost involved in site investigation studies. Hence, in this study, an attempt to characterize the sites was made using empirical methods logically modified to obtain optimum results. The study intended to predict the site classes at strong-motion stations along with comparing the accuracy of the different methods used. To encompass the regional site effects, HVSR, which is a stable indicator of site amplification, was used. The first method classified the stations based on the predominant period (obtained from the peak value of the HVSR curve) with a comparison to the JRA [40] recommended site-dependent period ranges. Within a station, different earthquakes gave different peak periods. The accuracy rate varied directly with the number of records given that the most recurring

predominant period value was assigned to each station. At some stations, there were no clear peaks and at times there were multiple peaks. Hence, it was difficult to ascertain the site class for some stations. The second method used was an empirical equation based on the peak parameters of HVSR to identify the  $V_{s30}$  value. The method was successful in predicting site classes C and D with a success rate of nearly 90%. Within a station, the site classes were mostly constant across all records. However, it could not identify most stations falling under classes A + B and E. The third and fourth method computed the correlation between the HVSR curve of a station and the standard HVSR curves. The averaged HVSR curves of the stations were correlated with HVSR curves given for K-net stations by Zhao et al. [16] and Alessandri et al. [17], respectively, in the methods. Site classes E and A + B could be easily identified. Additionally, Phung et al. [41] used for classifying the seismic stations considering the shape of the 5% damping PSA of horizontal ground components normalized with respective PGA value for site classification. This method classifies stations as either rock or soil. A single record could predict accurately the site class as it captures the response. The results matched mostly with the predominant-period-based classification. Variation of site class within a station was not more than one, which indicates that it is accurate as well as stable compared to previous methods. The final site class was assigned to each station after comparing the results obtained from each technique and assigning the most recurrent class. The initial and final set of stations of site classes shows a huge variation. The average HVSR response spectrum for each site class showed a low standard deviation of 0.3. Furthermore, the site classes were validated when compared to shear wave velocity profiles, results of topography-based studies, and spectral analyses. In comparison, it was found that using topographic maps for site classification is not effective at a regional scale, as the seismic site classification of stations in the Himalayan region varies considerably. Hence, empirical schemes using HVSR are excellent for site classification. These can be easily applied to classify a large number of stations. However, supplementary information from borehole data and shear wave velocity profiles may be used to validate the results. The HVSR curves can be sensitive to other parameters such as earthquake magnitude, focal depth, and source-to site distances. Hence, a model can be made for predicting the spectral ratios as a function of magnitude, distance, and site classification.

## Funding

This work was supported by the Science and Engineering Research Board (SERB), Department of Science and Technology, India [grant numbers SERB/F/162/2015–2016]. The authors extend their appreciation to International Scientific Partnership Program ISPP at King Saud University, Saudi Arabia for funding this research work through ISPP-040.

## References

- Nakamura Y. A method for dynamic characteristics estimation of subsurface using microtremor on the ground surface. *Q Report RTRI* 1989;30:25–33.
- Lachet C, Bard PY. Numerical and theoretical investigations on the possibilities and limitations of Nakamura's technique. *J Phys Earth* 1994;42:377–97.
- Lermo J, Chávez-García FJ. Site effects evaluation using spectral ratios with only one station. *Bull Seismol Soc Am* 1993;83:1574–94.
- Field EH, Jacob KH. A comparison and test of various site-response estimation techniques, including three that are not reference site dependent. *Bull Seismol Soc Am* 1995;85:1127–43.
- Bard YP. Microtremor measurements: a tool for site effect estimation? In the effects of surface. In: Irikura K, Kudo K, Okada H, Sataani T, editors. *Geology on seismic motion*. Rotterdam: Balkema; 1999. p. 1251–79.
- Bindi D, Parolai S, Spallarossa D, Cattaneo M. Site effects by H/V ratio: comparison of two different procedures. *J Earthq Eng* 2000;4:97–113.
- Nogoshi M, Igarashi T. On the amplitude characteristics of microtremor -Part 2 (in Japanese with English abstract). *J Seismol Soc Jpn* 1971;24:26–40.
- Arai H, Tokimatsu K. S-wave velocity profiling by inversion of microtremor H/V spectrum. *Bull Seismol Soc Am* 2004;94:53–63.
- Picozzi M, Albarello D. Combining genetic and linearized algorithms for a two-step joint inversion of Rayleigh wave dispersion and H/V spectral ratio curves. *Geophys J Int* 2007;169:189–200.
- Herak M. Model HVSR - a matlab tool to model horizontal-to-vertical spectral ratio of ambient noise. *Comput Geosci* 2008;34:1514–26.
- Ghofrani H, Atkinson GM. Site condition evaluation using horizontal-to-vertical response spectral ratios of earthquakes in the NGA-West 2 and Japanese databases. *Soil Dyn Earthq Eng* 2014;67:30–43.
- Bonnefoy-Claudet S, Cotton F, Bard YP. The nature of noise wavefield and its applications for site effects studies—a literature review. *Earth-Sci Rev* 2006;79:205–27.
- Bonnefoy-Claudet S, Cornou C, Bard PY, Cotton F, Moczo P, Kristek J, Fah D. H/V ratio: a tool for site effects evaluation. Results from 1-D noise simulations. *Geophys J Int* 2006;167:827–37.
- Yaghmaei-Sabegh S, Tsang H-H. A new site classification approach based on neural networks. *Soil Dyn Earthq Eng* 2011;31:974–81.
- Yaghmaei-Sabegh S, Tsang H-H. Site class mapping based on earthquake ground motion data recorded by regional seismographic network. *Nat Hazards* 2014;73(3):2067–87.
- Zhao JX, Irikura K, Zhang J, Fukushima Y, Somerville PG, Asano A, Ohno Y, Oouchi T, Takahashi T, Ogawa H. An empirical site-classification method for strong-motion stations in Japan using H/V response spectral ratio. *Bull Seismol Soc Am* 2006;96:914–25.
- Di Alessandro C, Bonilla LB, Boore DM, Rovelli A, Scotti O. Predominant period site classification for response spectra prediction equations in Italy. *Bull Seismol Soc Am* 2012;102(2):680–95.
- Nakamura Y. Clear identification of fundamental idea of Nakamura's technique and its applications. In: *Proceedings of the 12th world conference on earthquake engineering*, New Zealand; 2000.
- Lunedei E, Albarello D. Theoretical HVSR curves from full wavefield modelling of ambient vibrations in a weakly dissipative layered Earth. *Geophys J Int* 2010;181:1093–108.
- Bard Y, Theodulidis NP. Horizontal to vertical spectral ratios and geological conditions and analysis of strong motion data from Greece and Taiwan (smart – 1). *Soil Dyn Earthq Eng* 1995;14:177–97.
- Kobayashi H. Preliminary report on the ambient noise measurements in Thessaloniki, UNDP/SF, REM; 1973, p. 70–172.
- Scherbaum F, Riepl J, Bettig B, Ohnberger M, Cornou C, Cotton F, Bard PY. Dense array measurements of ambient vibrations in the Grenoble basin to study local site effects. *AGU Fall meeting*, San Francisco, December; 1999.
- Diagourtas D, Makropoulos K, Tzanis A. Comparative study of microtremor analysis methods. *Pure Appl Geophys* 2001;158:2463–79.
- Bonilla LF, Steidl JH, Lindley GT, Tumarkin AG, Archuleta RJ. Site amplification in the San Fernando Valley, California: variability of site-effect estimation using the S-wave, coda, and H/V methods. *Bull Seismol Soc Am* 1997;87:710–30.
- Stewart JP, Liu AH, Choi Y. Amplification factors for spectral acceleration in tectonically active regions. *Bull Seismol Soc Am* 2003;93(1):332–52.
- Di Giacomo D, Gallipoli Maria Rosaria, Mucciarelli Marco, Parolai Stefano, Richwalski Sandra M. Analysis and modeling of HVSR in the presence of a velocity inversion: the case of Venosa, Italy. *Bull Seismol Soc Am* 2005;95(6):2364–72.
- Borchardt RD. Estimates of site-dependent response spectra for design (Methodology and Justification). *Earthq Spectra* 1994;10:617–53.
- Abrahamson NA, Silva WJ. Summary of the Abrahamson & Silva NGA ground-motion relations. *Earthq Spectra* 2008;24:67–97.
- Akkar S, Sandikkaya MA, Bommer JJ. Empirical ground-motion models for point- and extended- source crustal earthquake scenarios in Europe and the middle east. *Bull Earthq Eng* 2014;12(1):359–87.
- Gregor N, Abrahamson NA, Atkinson GM, Boore DM, Bozorgnia Y, Campbell KW, Chiou BS-J, Idriss IM, Kamai R, Seyhan E, Silva W, Stewart JP, Youngs R. Comparison of NGA-West2 GMPEs. *Earthq Spectra* 2014;30:1179–97.
- Mahajan AK, Rob J, Sporry PK, Champati R, Rajiv R, Slob S, Cees Van W. Seismic microzonation of Dehradun City using geophysical and geotechnical characteristics in the upper 30 m of soil column. *J Seismol* 2007;11(4):355–70.
- Anbazhagan P, Sitharam TG. Mapping of average shear wave velocity for Bangalore region: a case study. *J Environ Eng Geophys* 2008;13(2):69–84.
- Boominathan A, Dodagoudar GR, Suganthi A, Uma Maheshwari R. Seismic hazard assessment of Chennai city considering local site effects. *J Earth Syst Sci* 2008;117(Suppl 2):853–63.
- Satyam ND, Rao KS. Seismic site characterization in Delhi region using the multi-channel analysis of shear wave velocity (MASW) testing. *Electron J Geotech Eng* 2008;13:167–83.
- Nath KS, Thingbaijam KKS. Assessment of seismic site conditions: a case study from Guwahati city, Northeast India. *pure. Appl Geophys* 2011;168:1645–68.
- Anbazhagan P, Kumar A, Sitharam TG. Seismic site classification and correlation between standard penetration test N value and shear wave velocity for Lucknow city. *Pure Appl Geophys* 2013;170:299.
- Lee CT, Tsai BR. Mapping Vs30 in Taiwan terrestrial. *Atmos Ocean Sci* 2008;19(6):671–82.
- Castellaro S, Mulargia F, Rossi PL. Vs30: proxy for seismic amplification? *Seismol Res Lett* 2008;79:540–3.
- Ghasemi H, Zare M, Fukushima Y, Sinaeian F. Applying empirical methods in site classification, using response spectral ratio (H/V): a case study on Iranian strong motion network (ISMN). *Soil Dyn Found Eng* 2009;29:121–32.
- Japan Road Association (JRA). Specifications for highway bridges Part V, Seismic design Maruzen Co., LTD; 1980.
- Phung V, Atkinson GM, Lau DT. Methodology for site classification estimation using strong ground motion data from the Chi-Chi, Taiwan, Earthquake. *Earthq Spectra* 2006;22(2):511–31.

- [42] Bilham R, Blume F, Bendick R, Gaur VK. Geodetic constraints on the translation and deformation of India: implications for future great Himalayan earthquake. *Curr Sci* 1998;74:213–29.
- [43] Kumar P, Yuan X, Ravi Kumar M, Rainer K, Xueqing L, Chadha RK. The rapid drift of Indian tectonic plate. *Nature* 2007;449:894–7.
- [44] Seeber L, Armbruster JG, Quittmeyer R. Seismicity and continental subduction in the Himalayan Arc. In: Zagros, Hindu Kush, Himalaya geodynamic evolution. In: Gupta HK, Delany FM, editors. *Geodynamics Series*, 4. Washington, DC: American Geographical Union; 1981. p. 215–42.
- [45] Khattri KN. Great earthquakes, seismicity gaps and potential for earthquake disaster along Himalaya plate boundary. In: Mogi K, Khattri KN, editors. *Earthquake prediction*, 138. *Tectonophysics*; 1987. p. 79–92.
- [46] Molnar P. A review of the seismicity and the rates of active underthrusting and deformation at the Himalaya. *J Himal Geol* 1990;12:131–54.
- [47] Bilham R, Gaur VK, Molnar P. Himalayan seismic hazard. *Science* 2001;293:1442–4.
- [48] Khattri KN, Wyss M. Precursory variation of seismicity rate in the Assam area, India. *Geology* 1978;6:685–8.
- [49] Srinagesh D, Singh SK, Chadha RK, Paul A, Suresh G, Ordaz M, Dattatrayam RS. Amplification of seismic waves in the central Indo-Gangetic Basin, India. *Bull Seismol Soc Am* 2011;101:2231–42. <https://doi.org/10.1785/0120100327>.
- [50] Singh IB. Geological evolution of Ganga plain – an overview. *J Paleontol Soc India* 1996;41:99–137.
- [51] Srivastava P. Palaeoclimatic implications of pedogenic carbonates in Holocene soils of the Gangetic Plains, India. *Palaeogeogr Palaeoclimatol Palaeoecol* 2001;72(3–4):207–22.
- [52] Sitharam TG, Govindaraju L. Geotechnical aspects and ground response studies in Bhuj earthquake, India. *Geotech Geol Eng* 2004;22:439–55.
- [53] Vishwa B, Chandel S, Kaur Brar K. Seismicity and vulnerability in Himalayas: the case of Himachal Pradesh, India. *Geomat Nat Hazards Risk* 2010;1(1):69–84.
- [54] Kumar A, Mittal H, Sachdeva R. Indian strong motion instrumentation network. *Seismol Res Lett* 2012;83(1):59–66.
- [55] Yamazaki F, Ansary M. Horizontal-to-vertical spectrum ratio of earthquake ground motion for site characterization. *Earthq Eng Struct Dyn* 1997;26:671–89.
- [56] Mittal H, Kumar A, Singh SK. Estimation of site effects in Delhi using standard spectral ratio. *Soil Dyn Earthq Eng* 2013;50:53–61.
- [57] Theodulidis NP, Bard YP. Horizontal to vertical spectral ratios and geological conditions: and analysis of strong motion data from Greece and Taiwan (SMART – 1). *Soil Dyn Earthq Eng* 1995;14:177–97.
- [58] Atkinson GM, Cassidy JF. Integrated use of seismograph and strong-motion data to determine soil amplification: response of the Fraser River delta to the Duvall and Georgia Strait earthquakes. *Bull Seismol Soc Am* 2000;90:1028–40.
- [59] Kanai K, Tanaka T. On microtremor VIII, *Bulletin of the Earthquake Research Institute*, 39; 1961, p. 97–114.
- [60] Fukushima Y, Bonilla LF, Scotti O, Douglas J. Site classification using horizontal-to-vertical response spectral ratios and its impact when deriving empirical ground motion prediction equations. *J Earthq Eng* 2007;11(5):712–24.
- [61] Luzi L, Puglia R, Pacor F, Gallipoli MR, Bindi D, Mucciarelli M. Proposal for a soil classification based on parameters alternative or complementary to Vs30. *Bull Earthq Eng* 2011;9(6):1877–98.
- [62] Seed HB, Ugas C, Lysmer J. Site-dependent spectra for earthquake-resistant design. *Bull Seismol Soc Am* 1976;66:221–43.
- [63] Iyengar RN, Ghosh S. Microzonation of earthquake hazard in greater Delhi area. *Curr Sci* 2004;87(9):1193–202.
- [64] Mukhopadhyay S, Pandey Y, Dharmaraju R, Chauhan PKS, Singh P, Dev A. Seismic microzonation of Delhi for ground-shaking site effects. *Curr Sci* 2002;82(7):877–80.
- [65] Singh SK, Mohanty WK, Bansal BK, Roonwal GS. Ground motion in Delhi from future large/great earthquakes in the central seismic gap of the Himalayan arc. *Bull Seismol Soc Am* 2002;92(2):55–569.
- [66] Nath SK, Sengupta P, Srivastav SK, Bhattacharya SN, Dattatrayam RS, Prakash R, Gupta HV. Estimation of S-wave site response in and around Delhi region from weak motion data, earth and planetary sciences. *Proc Indian Acad Sci* 2003;112(3):441–62.
- [67] Parvez I, Vaccari F, Panza GF. Site-specific microzonation study in Delhi metropolitan city by 2-d modeling of SH and P-SV waves. *Pure Appl Geophys* 2004;161:1165–85.
- [68] Pandey B, Ravi S, Jakka AK, Mittal H. Site characterization of strong-motion recording stations of Delhi using joint inversion of phase velocity dispersion and H/V curve. *Bull Seismol Soc Am* 2016;106(3):1254–66.
- [69] Wald DJ, Allen TI. Topographic slope as a proxy for seismic site conditions and amplification. *Bull Seismol Soc Am* 2007;97:1379–95.
- [70] Nath SK, Thingbaijam KKS, Adhikari MD, Nayak A, Devaraj N, Ghosh SK, Mahajan AK. Topographic gradient based site characterization in India complemented by strong ground motion spectral attributes. *Soil Dyn* 2013;55:233–46.